Research Square

Preprints are preliminary reports that have not undergone peer review.
They should not be considered conclusive, used to inform clinical practice,
or referenced by the media as validated information.

Foliar Graphene Sensor for Monitoring Intracellular and Extracellular Leaf Hydration Dynamics

Deji Akinwande

deji@ece.utexas.edu

University of Texas at Austin https://orcid.org/0000-0001-7133-5586

Ning Liu

University of Texas at Austin https://orcid.org/0000-0002-2187-5565

Pascal Ayelo

Texas A&M University

Utkarsh Misra

University of Texas at Austin

Maria Ulatowski

University of Texas at Austin

Caixing Xiong

Texas A&M University

Neelotpala Kumar

University of Texas at Austin

Michael Kolomiets

Texas A&M University

Henry Fadamiro

Texas A&M University

Jean Incorvia

University of Texas at Austin

Ashley Matheny

University of Texas at Austin

Dmitry Kireev

University of Massachusetts Amherst https://orcid.org/0000-0003-1499-5435

Article

Keywords:

Posted Date: May 18th, 2026

DOI: https://doi.org/10.21203/rs.3.rs-9597472/v1

License: This work is licensed under a Creative Commons Attribution 4.0 International License.
Read Full License

Additional Declarations: There is **NO** Competing Interest.

Foliar Graphene Sensor for Monitoring Intracellular and Extracellular Leaf Hydration Dynamics

Ning Liu[1], Pascal Mahukpe Ayelo[2,*], Utkarsh Misra[1,*], Maria Lynn Ulatowski[3], Caixing Xiong[2], Neelotpala Kumar[1], Michael Kolomiets[2], Henry Fadamiro[2], Jean Anne Incorvia[1], Ashley M. Matheny[3], Dmitry Kireev[4,&], and Deji Akinwande[1,5,&]

[1] Department of Electrical and Computer Engineering, University of Texas at Austin, Austin, Texas 78712, USA
[2] Department of Entomology, Texas A&M University, College Station, TX 77843
[3] Department of Earth and Planetary Sciences, The University of Texas at Austin, Austin, Texas 78712, USA
[4] Department of Biomedical Engineering, University of Massachusetts Amherst, Amherst, MA 01002, USA
[5] Department of Biomedical Engineering, University of Texas at Austin, Austin, Texas 78712, USA

[*] These authors contributed equally

[&] Corresponding authors: deji@ece.utexas.edu and dkireev@umass.edu

Abstract

Understanding plant water status and cellular hydration is fundamental to plant physiology, drought resilience, and precision agriculture. Yet current approaches infer hydration indirectly from soil moisture, microenvironmental conditions, or bulk tissue measurements, leaving the cellular water dynamics that govern physiological function largely inaccessible. In particular, no sensing platform enables *in vivo* differentiation between extracellular and intracellular water status in living leaves. Here, we present a foliar graphene sensor (FGS), a transparent, ultralight, breathable, and conformal atomic sensor. Unlike invasive metal electrodes that may damage tissue and hydrogel electrodes that can dehydrate over time, this foliar sensor enables non-invasive, continuous and multi-week quantitative monitoring of extracellular and intracellular water content in living plant leaves without disturbing physiological activity. By directly measuring the bioelectrical impedance spectrum of leaf tissue and incorporating the leaf as part of the sensing circuit, the device captures intrinsic plant hydration dynamics in real time. The sensing approach is broadly applicable across plant types and operational under natural outdoor conditions. *In vivo* measurements reveal that plants preferentially maintain intracellular water during dehydration–rehydration cycles, providing the first direct evidence of this physiological hierarchy in intact plants.

Main

Monitoring plant physiological processes and understanding water-response mechanisms are critical for both agricultural productivity and broader environmental resilience[1]. Among these processes, tracking leaf water content (LWC) is particularly important because leaves serve as the primary interface for water loss, gas exchange, and photosynthetic carbon assimilation. Compared with root, stem, or soil moisture indicators, leaf water status more directly reflects the plant's immediate physiological condition and stress responses. In agricultural systems, real-time monitoring of LWC, enables precision irrigation that reduces water use while sustaining or

improving crop yield[2]. Because stomata on leaves regulate transpiration and photosynthetic carbon assimilation, water deficits first manifest at the leaf level, where declines in turgor and stomatal conductance rapidly constrain growth and productivity. Beyond agriculture, LWC is a critical determinant of wildfire risk: leaves constitute the primary fine fuels, whose fuel moisture content (FMC) can change rapidly and strongly influences ignition potential and fire spread[3]. Consequently, leaf water status underpins metrics such as live fuel moisture and vegetation water content used in fire danger assessment, while also informing ecosystem health assessments[4] and climate change adaptation strategies[5]. Importantly, understanding how water redistributes between extracellular and intracellular compartments during dehydration–rehydration cycles can provide deeper insight into physiological strategies used by plants to maintain cellular hydration under water stress. Achieving these capabilities requires continuous, long-term monitoring of LWC in living plants.

Despite the recognized importance of leaf water status, long-term, non-invasive monitoring in living plants remains challenging. Existing approaches span a trade-off between accuracy and invasiveness: indirect methods such as soil moisture sensing or transpiration-based estimation are non-destructive but are often imprecise to reflect true plant hydration status[6–8] (Figure 1a), whereas gravimetric analysis provides precise quantification but requires destructive sampling[9–12]. Electrode-based electrophysiological monitoring enables direct interrogation of plant tissues but presents additional limitations. Invasive metal probes inserted into stems can cause permanent tissue damage and alter physiological responses[13]. Although microneedle electrodes reduce injury, their application is typically restricted to stems, petioles, or thick leaves to ensure mechanical stability and tolerance to micro-injury[14]. These challenges are particularly acute for soft, delicate leaves, whose electrical and optical properties are closely linked to photosynthesis and stress signaling, yet are incompatible with insertion-based approaches and difficult to monitor reliably over extended periods. Wet electrodes provide conformal contact and remain the gold standard for short-term measurements; however, dehydration limits their operational lifetime to less than a few days, and rehydration often introduces instability and poor reproducibility[15]. (Table 1, Note S1) Among electrical approaches capable of longer-term monitoring, methods based on relative humidity in the leaf microenvironment do not involve electrical current passing through the leaf tissue and therefore provide only indirect estimates of LWC[6,16–18]. In our previous work, we developed transistor-based sensors integrated directly on leaves for hydration monitoring[19]; although the sensing current traversed the leaf tissue, the measured response reflected the bulk electrical properties of the leaf and could not resolve contributions from distinct tissue compartments. Importantly, fully understanding plant water dynamics requires longer term continuous measurements across repeated dehydration–rehydration cycles, during which leaf tissues undergo rapid and heterogeneous redistribution of water. As a result, existing approaches do

not provide real-time, long-term, non-invasive measurements of LWC or resolve tissue-level hydration dynamics in intact plants. Bridging this gap requires a sensing strategy that is mechanically compliant, physiologically compatible, and capable of stable, long-term operation on living leaves.

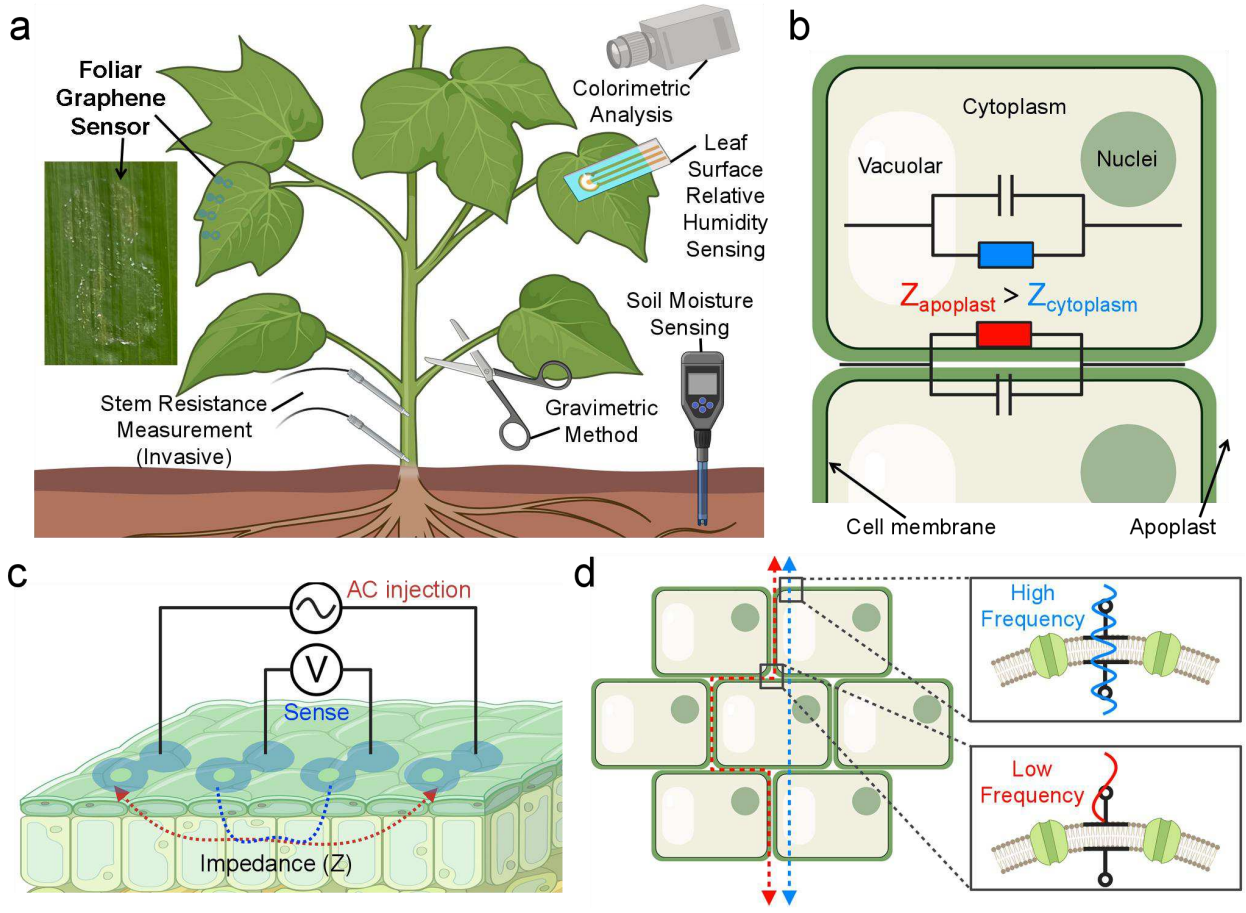


Figure 1. Working principle of foliar graphene sensors (FGS) for monitoring plant hydration status. ***a,*** *Overview of representative techniques for measuring plant water content. The top-left highlights the FGS approach developed in this work, together with optical images showing a transparent graphene sensor conformally attached to the corn leaf.* ***b,*** *Simplified equivalent circuit model of current flow through leaf tissue illustrating the transport routes through the intracellular compartment of mesophyll cells and through the apoplastic space.* ***c****, Schematic illustration of the four-probe bioimpedance measurement principle. Four graphene electrodes are placed in parallel on a leaf surface to enable electrochemical impedance spectroscopy, allowing direct measurement of internal tissue impedance.* ***d****, Schematic depiction of frequency-dependent current pathways through leaf tissues. Red arrows depict low-frequency alternating current, which mainly travels through extracellular (apoplastic), whereas blue arrows represent high-frequency current, which penetrates cell membranes and flows through both extracellular and intracellular (cytoplasm).*

A strategy capable of resolving distinct conduction pathways within living leaves is therefore needed. Bioelectrical impedance spectroscopy (BIS) enables depth-selective interrogation of biological tissues through frequency-dependent electrical currents[20], providing a route to probe hydration dynamics within intact leaves. Here, we present a FGS that incorporates the leaf tissue itself into the electrical current pathway, enabling direct interrogation of tissue hydration (Figure 1c). By analyzing impedance responses across excitation frequencies, the FGS distinguishes extracellular and intracellular conduction pathways, enabling compartment-resolved quantification of LWC *in vivo*. The ultrathin sensor accommodates natural leaf growth and motion while maintaining optical transparency (>97%) and gas permeability, key properties that have made graphene widely used for flexible bioelectronic interfaces[21–25], hence, affording continuous measurements for more than two weeks, substantially longer than most hydrogel-based electrodes. Because this approach relies on fundamental electrical properties of plant tissues and a conformal, breathable interface, it is not restricted to a specific plant species and can be applied to leaves with different morphologies. This foliar graphene sensing platform provides a unique approach for resolving hydration dynamics in living leaves and enables direct assessment of plant water stress (Note S2), opening new opportunities for advancing plant physiological research and elucidating drought-resilience mechanisms under water stress.

Table 1. Benchmarking against prior state-of-the-art studies.[7,14,16,26,27,19,15,17] ***LWC, leaf water content; RH, relative humidity; PW, plant water potential; DC, direct current.***

Study	Measured Quantity	Measured Method	Transparent and Flexible	Breathable	Current Path	Intra-/Extracellular Water Differentiation
This Work	LWC	4-Probe Impedance		Yes	Trans-leaf	Yes
[7]	LWC			No	Trans-leaf	No
[16]	RH	2-Probe Impedance		No	Near-leaf	No
[26]	PW and RH			Yes	Near-leaf	No
[27]	LWC			Yes	Trans-leaf	No
[14]	PW			Yes	Trans-leaf	No
[19]	LWC	2-Probe Conductance		Yes	Near-leaf	No
[15]	PW	Capacitance		Yes	Near-leaf	No
[17]	RH	DC Resistance		Yes	Near-leaf	No

Non-Flexible & Transparent | Flexible & Transparent | Non-Flexible & Non-Transparent | Flexible & Non-Transparent

Sensing Principle for Resolving Intracellular and Extracellular Water

To achieve accurate and reliable BIS measurements of leaf tissue, the sensing current must penetrate the mesophyll tissue rather than superficial features such as rigid trichomes, epidermal cells, or surface contaminants (e.g., dust or wax layers). This is accomplished by positioning two pairs of FGS electrodes in parallel on the leaf surface at equal spacing. The outer electrode pair injects an alternating current (AC) into the leaf, while the inner pair records the resulting bioimpedance response (Figure 1c). This configuration is analogous to the four-probe (Kelvin) method which is used to eliminate contact resistance in electronic materials characterization[28]. By decoupling the current injection and voltage sensing pathways, the four-electrode arrangement separates contact impedance from the intrinsic impedance of the mesophyll tissue, which is sensed exclusively by the inner electrode pair. Consequently, the measured impedance predominantly reflects the intrinsic electrical properties of the leaf tissue rather than electrode–leaf interface resistance.

The frequency of the applied AC signal plays a critical role in determining the electrical current pathways within plant tissues. The lipid bilayers of cell membranes behave as dielectric layers that create capacitor-like interfaces[29]. Consequently, at low frequencies, current cannot

readily traverse the membrane to reach the intracellular space, and the measured impedance primarily reflects resistance from the apoplast (Figure 1d). Under these conditions, current flows predominantly through intercellular spaces within the loosely arranged spongy mesophyll beneath the leaf surface. As the excitation frequency increases, capacitive reactance decreases, enabling capacitive coupling across the membrane and allowing current to access intracellular compartments. Once the membrane barrier is effectively bridged, current preferentially flows through intracellular domains. Compared with the apoplast, intracellular compartments exhibit higher electrical conductivity; in particular, cytoplasmic conductivity[30] ($\sigma \approx 0.5–2\ S \cdot m^{-1}$) is often higher by several-fold than that of extracellular fluids in leaf tissues depending on ionic composition[31] (Figure 1b). Consequently, the dominant current pathway shifts to conduction through mesophyll cell interiors. Collectively, this frequency-dependent behavior enables selective probing of extracellular and intracellular water compartments, providing a direct signature of leaf hydration dynamics.

Foliar Graphene Sensor Bioimpedance Measurement Strategy and Readout

Because the sensors reported in this study directly interface with the leaf tissue to sense the water content dynamics of the leaf, sensor placement is critical for obtaining physiologically meaningful measurements. To evaluate positional effects, impedance was measured at multiple locations on maize leaves, including the adaxial (top), abaxial (bottom), across individual leaf (transverse), and between leaves (Figure 2a, Figure S8). Impedance was consistently lower on the abaxial surface. This observation aligns with leaf anatomical and physiological asymmetry: the abaxial side typically exhibits higher stomatal density and greater transpiration, resulting in elevated local humidity and enhanced ionic conductivity. In C_4 plant species such as maize, stomatal density is typically higher on the abaxial than on the adaxial leaf surface[32]. This structural and functional asymmetry governs directional water flux and gas exchange, making abaxial impedance measurements particularly informative. Since current preferentially follows through ionic pathways within hydrated tissue, impedance changes on the abaxial side provide a direct and sensitive indication of fluctuations in leaf hydration and transpiration dynamics, thereby offering a reliable proxy for assessing, *in vivo,* water status. Guided by both impedance mapping and leaf physiological structure, sensors were therefore positioned on the abaxial surface in subsequent experiments.

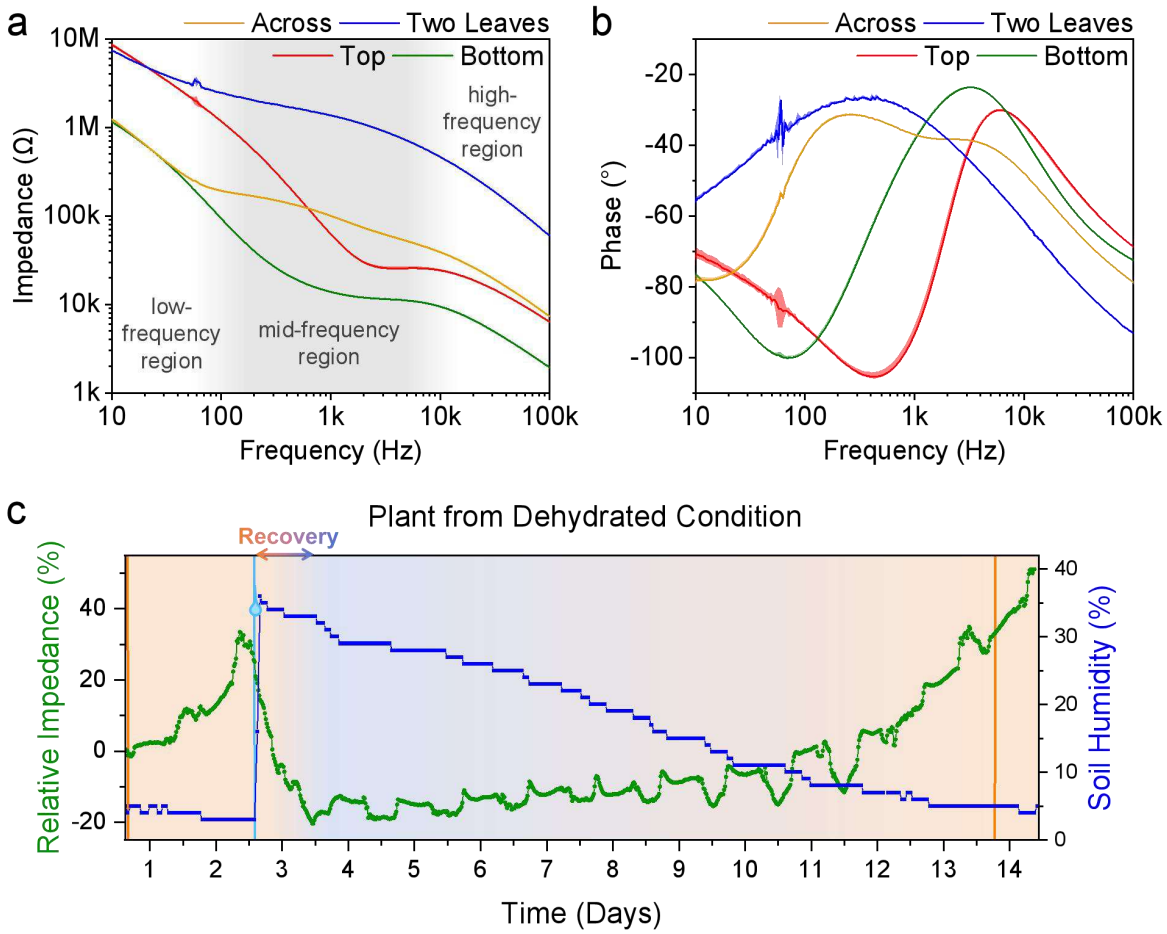


Figure 2. Fundamental characteristics and physiological signals measured by the FGS. ***a****, Impedance-frequency plot at different positions of FGS on leaves (n = 6 sensors per group). The solid lines represent the mean; the coefficient of variation (CV) is 0.86%.* ***b****, Phase-frequency plot acquired simultaneously from the same set of sensors as in* ***a****. The solid lines represent the mean; the CV is 0.68%.* ***c****, Relative impedance ($\Delta Z/Z_0$ at 1kHz) and soil humidity curves for a corn plant from dehydrated condition, monitored over a 14 day period, showing a Pearson correlation coefficient of r = -0.7 between impedance and soil moisture. The water drop icon indicate irrigation event, while orange vertical lines denote the onset of visually detectable water stress (leaf curling). Semitransparent orange and blue backgrounds represent periods of water stress and hydrated, respectively. A rapid impedance response is observed immediately after irrigation, followed by roughly one day of recovery (Figure S11). The x-axis shows time in days, with each day starting at midnight.*

As described earlier, low-frequency current predominantly travels through extracellular pathways, whereas high-frequency current increasingly accesses intracellular compartments. This frequency-dependent redistribution of current pathways is most evident in sensors placed across the leaf (two electrodes on the adaxial and two on the abaxial surfaces, Figure 2a,b),

where the measured response represents a composite of both surfaces. In monocot C_4 plants such as maize, the abaxial side is dominated by spongy mesophyll, where loosely arranged cells and large intercellular spaces facilitate ionic conduction. In contrast, the adaxial surface contains more tightly packed palisade cells with thicker cell walls, presenting higher resistance to extracellular current flow. Consequently, the across-leaf response at low frequencies resembles that measured on the abaxial surface. As frequency increases and capacitive coupling across cell membranes strengthens, current increasingly penetrates intracellular domains. Water-rich intracellular compartments provide comparatively low-resistance pathways that promote intracellular conduction. Under these conditions, the across-leaf response shifts toward that of the adaxial measurement. In the mid-frequency regime, contributions from extracellular and intracellular pathways overlap, producing an intermediate response that reflects the combined electrical behavior of both tissue domains. Based on the spatial impedance responses observed across leaf locations, three frequency regimes can be distinguished: a low-frequency region dominated by extracellular conduction, a mid-frequency region reflecting mixed extracellular–intracellular contributions, and a high-frequency region dominated by intracellular conduction (Figure 2a).

With this configuration, continuous and reliable impedance measurements were obtained across the full frequency range (10 Hz–100 kHz) throughout the two-week monitoring period (Figure S15). Because impedance magnitude varies substantially with frequency due to the frequency-dependent permeability of plant tissues[33], examining representative frequencies more clearly reveals hydration-related fluctuations (Figure 2c). We therefore focus on the mid-frequency regime (1 kHz shown as a representative example; Note S3), where both extracellular and intracellular components contribute to the signal, providing an integrative measure of leaf hydration state.

Distinct impedance responses were observed following irrigation of drought-stressed plants, with well-watered controls included for comparison in the Supplementary Information (Figure S11). Impedance monitoring was initiated when plants were already severely water-deficient and exhibited visible leaf curling. In these drought-stressed plants, the initial impedance was markedly elevated (Figure 2c). Following irrigation, a rapid electrical response was observed immediately: within approximately 20 minutes of watering, impedance dropped sharply, indicating rapid uptake and transport of water into leaf tissues. Over the subsequent hours, impedance continued to decrease as hydration progressed, ultimately returning to pre-stress levels within ~24 hours and stabilizing at a low baseline level for several days (Figure 2c). This progressive decline in impedance coincided with visible physiological recovery, including leaf unfolding and restoration of normal diurnal rhythms. Such delayed recovery is consistent with prior studies showing that severe or prolonged drought slows recovery of leaf water status and gas exchange relative to well-watered plants[34,35] (Figure S12). In the absence of further

irrigation, impedance gradually increased again, reflecting progressive dehydration of leaf tissue and completing a subsequent hydration–dehydration cycle. Notably, a measurable increase in impedance occurred up to two days before visible leaf curling (orange line), indicating that water stress begins well before external symptoms appear. By directly measuring leaf water status, the FGS enables timely irrigation prior to visible stress onset. Such early intervention is critical for maintaining plant function: once curling becomes evident, rehydration and physiological recovery typically require ~24 hours, whereas pre-symptomatic irrigation restores water balance within a few hours (Figure S12). Anticipatory irrigation therefore sustains physiological activity while avoiding excessive water use, supporting both crop productivity and sustainable resource management (Figure S14). This impedance measured hydration–dehydration cycle closely paralleled trends in soil moisture content (Figure S13). However, soil moisture alone does not directly reflect plant water status, highlighting the need for a physiological calibration that directly relates impedance measurements to leaf tissue hydration.

Resolving Leaf Tissue Hydration and Rehydration Dynamics from Bioimpedance

Our objective is to quantify hydration within leaf tissues, specifically the water content of mesophyll cells and the extracellular space. To establish this physiological link, impedance was correlated with LWC, a standard physiological metric that normalizes differences in leaf size and mass and is widely used to assess relative hydration status, particularly during drought stress and recovery. Impedance and LWC were measured simultaneously, enabling direct calibration (Figure S9). As shown in Figure 3a, impedance values across all measured frequencies exhibited strong correlations with LWC, confirming impedance spectroscopy as a quantitative reporter of LWC. Notably, the impedance–LWC relationship was consistently described by an exponential function across the full frequency spectrum, with frequency-dependent fitting parameters. This shared functional form suggests a common biophysical mechanism linking tissue hydration to ionic conduction pathways. This calibration further enables reconstruction of extracellular and intracellular water content over time (Figure 3b, Figure S10), validating impedance sensing as a non-destructive approach for resolving tissue-specific hydration dynamics with high temporal resolution.

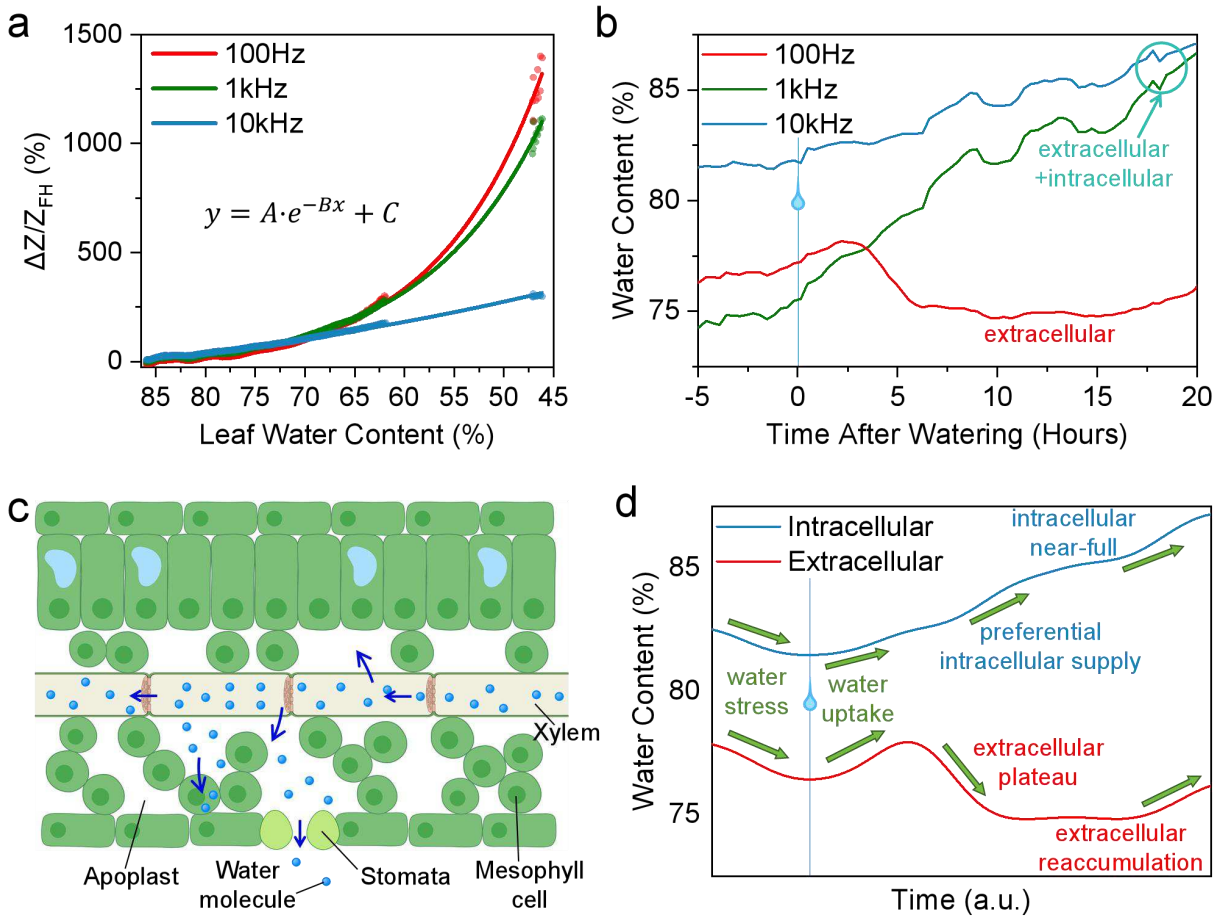


Figure 3. Relationship between impedance and LWC. ***a****, Correlation between impedance and LWC. The relationship between impedance at various frequencies and LWC was established using the gravimetric LWC method, which quantifies hydration based on mass loss after drying. Solid lines represent the fitted curves, scatter points indicate the measured data.* Z_{FH} *denotes the impedance under fully hydrated conditions.* ***b****, Water content changes in extracellular and intracellular compartments around irrigation. The water content in different tissues was calculated by impedance–LWC correlation, spanning 5 hours before to 20 hours after irrigation.* ***c,*** *Schematic illustration of water transport in a plant leaf. Water moves from the xylem vessel across the vessel wall into the extracellular space (apoplast). It is subsequently partitioned between uptake into mesophyll cells (intracellular compartment) and transpiration to the atmosphere through the stomata.* ***d,*** *Schematic of extracellular and intracellular water content dynamics before and after irrigation.*

Having established a quantitative framework for reconstructing intracellular and extracellular water content, we next examined how water is transported into and redistributed within leaf tissues during rehydration. Following irrigation, drought-stressed plants absorb water through the roots, which is transported upward through the xylem conduits of the leaf veins. Water then moves radially across the vessel walls through pit membranes into the cell wall matrix and

intercellular spaces, collectively forming the apoplast (extracellular compartment). Subsequently, water crosses the plasma membrane and enters mesophyll cells, replenishing intracellular water stores (Figure 3c).

Given the exponential relationship between impedance and LWC, Figure 3b presents the temporal evolution of water content within intracellular and extracellular compartments following irrigation. Under fully hydrated conditions, water content in both compartments exceeds approximately 85% (Figure 3a). Under drought stress prior to irrigation (Figure 3b), intracellular compartments retain a higher water fraction than extracellular regions, indicating that plants preferentially preserve intracellular hydration during water deficit. Within approximately 20 minutes of watering, impedance drops sharply, reflecting rapid water uptake and transport into leaf tissues. In drought-stressed plants, this rapid response is observed across both high and low frequencies, indicating simultaneous replenishment of extracellular and intracellular water pools. Following this initial uptake, intracellular water content continues to increase steadily. In contrast, extracellular water content rises rapidly but then temporarily declines, suggesting redistribution of water from the apoplast into cells. Once intracellular nears full hydration (~85%), extracellular water levels rise again. These results indicate that maize plants preferentially allocate absorbed water to intracellular compartments to restore cellular turgor and metabolic function, while the extracellular space functions as a transient transport and buffering reservoir.

Physiological Compatibility of the Foliar Graphene Sensor

Building on this sensing mechanism, direct electrical coupling between the FGS and plant tissue, enables probing of intrinsic plant properties and yields physiologically relevant signals. However, such intimate contact raises a critical question: whether the sensing interface perturbs normal physiological processes.

To evaluate the optical compatibility of the FGS, leaf pigmentation was monitored as a non-invasive indicator of plant physiological status. Because leaf pigmentation reflects chlorophyll accumulation and photosynthetic activity[36], changes in coloration provide a convenient proxy for assessing potential sensor-induced effects on leaf development. A graphene patch was applied to the second uppermost (newly matured) leaf of the corn plant during the V5–V8 rapid growth stage, and its effect was assessed by comparing the color difference between the patch-covered region and an adjacent reference area (Figure 4a). A control sample using a medical-grade Tegaderm film, selected for its widely cited biocompatibility and transparency, was included for comparison. Both graphene and control patches were monitored over a two-week period, and changes in leaf pigmentation were

quantified using vector-based color analysis (Note S4). Graphene's high optical transmittance (up to 97%)[37] minimizes interference with photosynthetically active radiation reaching the leaf. In contrast, although Tegaderm is transparent, it partially attenuates light in the photosynthetically active spectral range (400 – 700 nm). This distinction is visually evident in Figure 4a; leaves covered with graphene deepen in green coloration as they grow, mirroring the normal development of uncovered leaves, whereas Tegaderm-covered regions showed markedly reduced color deepening. This diminished greening suggests reduced chlorophyll accumulation under the film, indicating suppressed photosynthetic activity. In contrast, graphene-covered regions exhibited normal progressive darker greening during leaf growth, indicating that the FGS does not interfere with chlorophyll accumulation or normal leaf development.

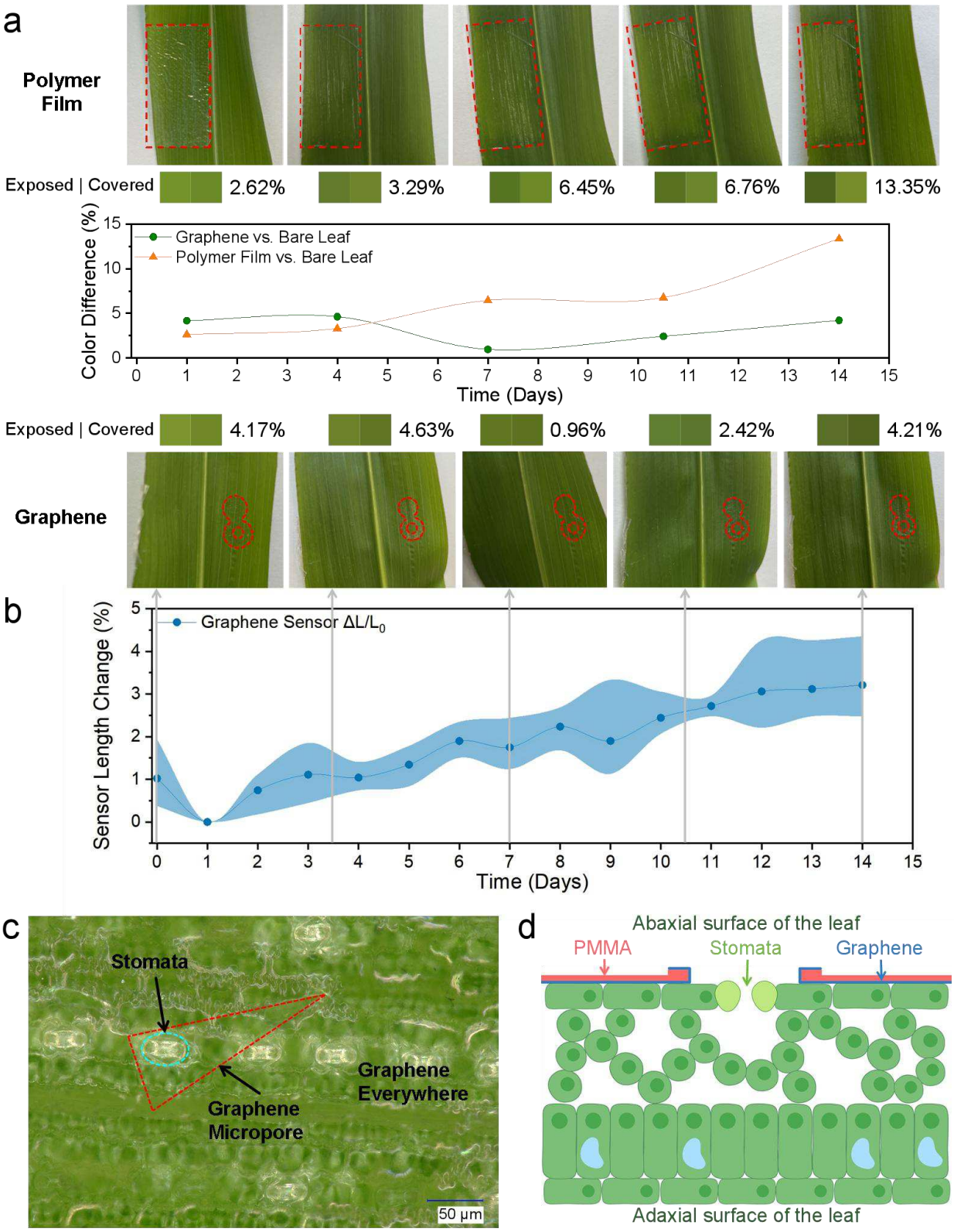


***Figure 4. Plant growth and physiological activity remain unaffected by FGS. a**, Leaf color change. The top row shows time-lapse images of a polymer film placed on a corn leaf, while the bottom row shows the corresponding images for FGS. The central color bar compares the original leaf color (left) with the*

covered area color (right, graphene or polymer film), with percentages indicating the relative color difference (Note S4). The middle plot quantifies the temporal evolution of this color difference. ***b****, FGS growth with the leaf. The length of FGS attached to corn leaves (n = 3) was measured over 14 days. The solid line represents the mean, and semitransparent area represent the range between the maximum and minimum values. The sensor length at day 1 was used as the reference (0%) because measurements at day 0 were conducted immediately after water-assisted transfer, when the FGS was elongated relative to its dry state (the observed first day shrinkage).* ***c****, Micropores on FGS. Optical micrograph of a FGS attached to a leaf surface. Triangular micropores (exposed leaf areas without graphene, Figures S5 and S6) are outlined with red dashed lines, and a native leaf stomatal pore is marked with a red dashed ellipse. The surrounding regions outside the triangular opening are covered by graphene.* ***d****, Schematic of graphene micropore and leaf stomata alignment showing a cross-sectional view of a leaf with a stomatal pore, and the FGS conformally attached to the abaxial (lower) surface.*

Equally important is mechanical compatibility. As plant leaves grow, elongate, and respond dynamically to environmental cues such as water availability and light cycles, the sensor must accommodate these morphological changes without detachment or signal degradation. The ultrathin nature of graphene allows conformal contact with the leaf surface, while its intrinsic stretchability (~15%)[38] enables the sensor to elongate alongside natural leaf expansion. Mechanical compliance was further improved through a donut-shaped design that minimizes strain concentration[23]. Over a continuous two-week monitoring period during the rapid growth stage of corn, the sensor accommodated an average elongation of 3.2 ± 1% due to leaf growth (Figure 4b), yet maintained stable impedance readings throughout, demonstrating robust mechanical resilience and electrical reliability under active growth conditions. Moreover, the ultrathin (<0.3 μm electrode thickness, ≈10 μm total) and lightweight (<0.1 mg electrode weight, <0.3 g complete setup; Note S2,S3) configuration imposed negligible load on the leaf, preserving its posture and growth behavior.

Finally, to preserve the leaf's gas exchange function, which is crucial for both photosynthesis and transpiration, microporosity was introduced into the graphene film. These micron-scale pores ensure sufficient air permeability (Figure 4c,S5,S6), maintaining natural leaf-atmosphere gas exchange across the contact interface. This design strategy draws inspiration from recent advances in epidermal electronics, where similar microporous graphene structures have demonstrated long-term biocompatibility on human skin for continuous biosensing, with water vapor transmission rates (WVTR) of approximately 2770 g m^{-2} day^{-1}, comparable to open surfaces (~3600 g m^{-2} day^{-1}), thereby confirming that microporosity effectively preserves gas permeability[39]. By adapting this concept to plant surfaces, we achieve a non-invasive, physiologically inert interface that enables long-term monitoring without disrupting photosynthesis, growth processes, or gas exchange.

The ability to maintain long-term, non-invasive contact with the leaf surface further enables deployment beyond controlled laboratory settings and across different plant species (Figure 5). The ultrathin, conformal graphene interface forms stable electrical coupling with leaves of different surface morphologies and mechanical properties, including monocot and dicot leaves as well as thicker woody leaves, enabling the sensor to be interfaced with a range of plant species, such as maize, cotton, and red oak (Figure 5a–d). Notably, stable measurements were obtained under fully outdoor conditions over multiple days (Figure 5e), during which leaves were exposed to natural environmental fluctuations such as wind, temperature, and light cycles. These results indicate that the FGS is not restricted to a specific plant species and is compatible with long-term, non-invasive, in situ monitoring under realistic environmental conditions.

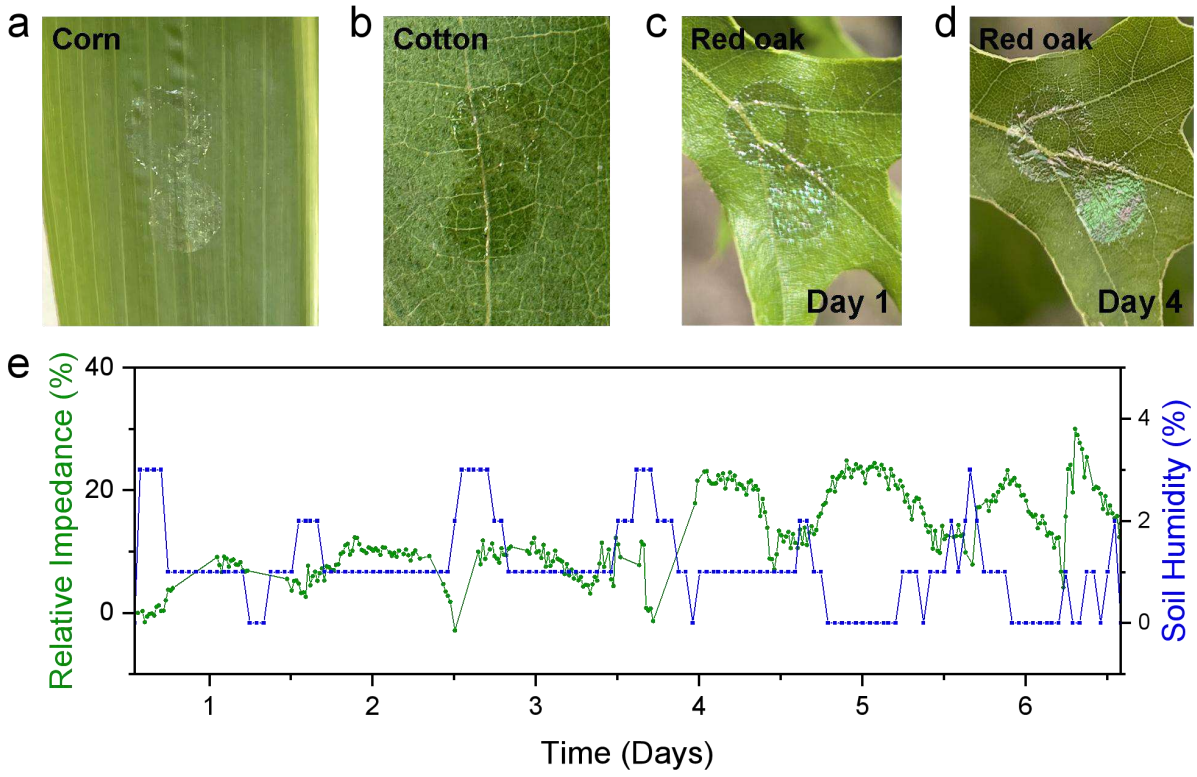


Figure 5. Cross-species applicability of FGS and outdoor field validation. a*, FGS conformally attached to a corn leaf in the laboratory.* ***b****, FGS conformally attached to a cotton leaf in a greenhouse.* ***c****, FGS attached to a red oak (Quercus buckleyi) leaf under outdoor conditions (day 1) and at* ***d****, day 4.* ***e****, Continuous impedance and soil moisture measurements recorded over six days under outdoor conditions (Note S7), showing a Pearson correlation coefficient of r = -0.6 between impedance and soil moisture.*

Conclusion

In summary, we introduce the foliar graphene sensor, a bioimpedance sensing platform that enables, for the first time, non-invasive and long-term quantification of intracellular and extracellular water content in living leaves without perturbing plant physiology. The ultrathin, ultralight, graphene interface forms a stable and physiologically compatible coupling with leaf tissue, enabling continuous monitoring of compartment-specific hydration dynamics. This capability reveals a previously unobserved rehydration strategy in plants: during water deficit and recovery, intracellular hydration is preferentially preserved and restored, while the extracellular space functions as a transient transport and buffering reservoir. By providing direct electrical access to tissue-level water dynamics, FGS further enables detection of physiological drought stress up to two days before visible leaf curling.

Beyond advancing fundamental understanding of plant water regulation, FGS provides a quantitative tool for investigating tissue-level hydraulic dynamics, cellular turgor regulation, and stress adaptation mechanisms in living plants. As this approach relies on fundamental electrical properties of plant tissues and a conformal, physiologically compatible interface, it establishes a general platform for long-term, *in situ* monitoring of plant hydration dynamics in realistic environments. By affording direct, non-destructive tracking of compartment-specific hydration, this platform opens new opportunities to study plant responses to drought, heat, and salinity, as well as dynamic water transport under fluctuating environmental conditions. These mechanistic insights further support the development of precision irrigation strategies and distributed environmental sensing and may ultimately inform ecosystem-scale assessments such as live fuel moisture monitoring for wildfire risk prediction.

Materials and Methods

Fabrication of Foliar Graphene Sensor

Graphene requires adequate protection and support, provided using the ultrathin layer of PMMA. High-quality monolayer graphene was grown via the chemical vapor deposition (CVD) method on a copper foil (Grolltex). The graphene/copper piece was fixed on a Si wafer by the Kapton tape. A layer of PMMA (950 A4) was spin-coated at 2500 rpm for 60 seconds and baked at 200 ℃ on a hotplate for 20 minutes. The copper was removed by placing the PMMA/graphene/copper in 0.1 mol $(NH_4)_2S_2O_8$ solution for 8–12 hours. The floating PMMA-graphene was then picked up by a Si wafer and transferred into deionized (DI) water to remove any residual copper etchant solution. The PMMA/graphene piece was then picked up by a new piece of clean 1-layer graphene/copper. The PMMA-graphene-graphene-copper was air-dried overnight at room temperature in a hood. The 2-layer graphene was produced by annealing the PMMA-graphene-graphene-copper on a hot plate at 200 °C. The copper foil of the 2-layer graphene was also removed by immersion in 0.1 mol $(NH_4)_2S_2O_8$ solution for 8–12 hours. Transferred the PMMA/graphene using two sheets of tattoo paper (Silhouette Cameo) and flipped the structure to have an arrangement with graphene facing up.[21] The graphene on tattoo paper was attached to Silhouette Cameo cutting mat using the Kapton tape. A Cameo plotter was used to cut the graphene into "8" shapes.

Fabrication of Gold Tape and Wired Contacts

Gold tape electrodes were fabricated on an ultrathin adhesive polymer substrate (ISR-BSMK10G, Iwatani). A 10-nm nickel (Ni) adhesion layer followed by a 60 – 90 nm gold (Au) layer was deposited by electron-beam evaporation (PVD75). The gold tape was then cut into strips using a plotter cutter (Silhouette Cameo).

Electrical leads were formed by attaching enameled copper wires (36 AWG, BENTECHGO) to the gold strips (4 mm × 30 mm) using conductive silver epoxy (8331S, MG Chemicals). The epoxy was applied only to the overlap region (~4 mm) between the wire and the electrode to minimize mechanical stiffness. Assemblies were cured at room temperature for 72 h before use.

Plant Material and Growth Conditions

The drought-sensitive corn (Zea mays) cultivar CML 176 was used in this study. Seeds were sown and grown in a greenhouse under ambient environmental conditions without active control of temperature, humidity, or light beyond standard greenhouse operation. After 4 – 5 weeks of growth, plants reached the 5–6 leaf stage, at which point all experimental measurements were initiated. During the subsequent 1–2 weeks of monitoring, plants reached 5–7 weeks of age.

Unless otherwise specified, impedance measurements were performed under ambient laboratory conditions. Additional experiments conducted under controlled illumination and natural outdoor environments are described in the Supplementary Information.

Sensor Placement and Bioimpedance Measurement

The FGS were positioned on the plant leaf lamina while avoiding the midrib, with one end making direct contact on the leaf epicuticular, and the other end covering a portion of an adhesive, elastic, and conductive gold tape (10 µm thickness, 4 mm in width, ~30 mm in length) placed on the leaf (Supplementary Video 1). To enhance mechanical stability, particularly under outdoor conditions with wind, a small piece of Tegaderm film can be applied at the distal end of the gold tape to further secure the interconnect to the leaf surface. The second end of the gold tape bearing a thin wire (36 AWG Enameled Copper Wire, BENTECHGO) was connected to the measuring electronics on the LCR (L: inductance, C: capacitance and R: resistance) meter (IM 3536, Hioki, Japan). The excitation signal was set to a constant 0.05 V with a current limit of 0.0001 A. The plant bioimpedance was recorded under both watered and water-stressed conditions, by mounting the FGS on the first top developed leaf, as studies on LWC in corn revealed that the LWC in the top leaf is most representative of the plant water status[40]. Measurements were performed under a wide range of frequencies (10–100,000 Hz) to capture the electrical properties of both intracellular and extracellular environments[41].

Impedance Data Processing

Impedance data were recorded using the LCR meter and exported for analysis. Python was used to extract impedance values at 1000 Hz at different time points (Note S3). Environmental measurements were aligned with impedance recordings using timestamp matching.

Environmental Monitoring during Hydration–Dehydration Experiments

During impedance measurements, environmental and soil parameters were recorded concurrently. Soil humidity (%), ambient light (mmol), temperature (°C), and soil electronic conductance (µS/cm) were measured using a commercial soil sensor (Flower Care™ Smart Monitor) inserted into the soil approximately 2 cm from the base of the plant. Measurements were automatically logged at hourly intervals using the accompanying software. Relative humidity (%) was recorded using a commercial thermo-hygrometer at the same hourly intervals.

Soil moisture was used as a proxy for available soil water content (ASWC)[42]. and was compared with impedance measurements to evaluate the temporal relationship between soil drying, onset of water stress, and changes in plant hydration status (Figure S13) .

Impedance–LWC Calibration during Controlled Leaf Dehydration

To establish a quantitative relationship between impedance and LWC, detached leaves were allowed to dehydrate under ambient laboratory conditions while impedance was monitored. Leaves were placed on a precision balance (Sartorius Entris II BCE124-1S Analytical Lab Balance)

to record mass continuously, and impedance measurements were performed at predefined time intervals throughout dehydration. At each impedance measurement time point, the corresponding leaf mass was obtained from the balance record to determine fresh mass. After completion of the dehydration monitoring period (up to 4 days), leaves were oven-dried at 70 ° C for 48 h to obtain dry mass. Water mass was calculated as the difference between fresh and dry mass, and percent LWC was calculated by normalizing water mass to the fresh mass.

Leaf water content was calculated as:

$$\mathrm{LWC}\ (\%) \ = \ \frac{M_{\mathrm{total}} \ - \ M_{\mathrm{sensor}} \ - \ M_{\mathrm{dry}}}{M_{\mathrm{total}} \ - \ M_{\mathrm{sensor}}} \ \times \ 100$$

Data Analysis

Data visualization and curve fitting were performed using Origin and Python. Correlative analyses and heatmap generation were conducted in Python (Note S6). The full correlation matrix between impedance and environmental variables is provided in Supplementary Figure S16.

Statistical Analysis

Sample sizes (n) refer to independent biological replicates and are reported in figure legends. Data are presented as the mean, with shaded regions indicating the minimum–maximum range unless otherwise noted. Details of statistical analyses are provided in the Supplementary Information.

Code Availability

The custom Python scripts used for data processing and analysis in this study are available at GitHub (https://github.com/rua-maomao/FGS-data-processing).

Acknowledgements

D. Akinwande acknowledges the Cockrell Family Regents Chair, and N. Liu was supported in part by a UT-Portugal Grant.

Author Contributions

D.A. conceived the idea. D.K. and N.L. designed the foliar graphene sensors with N.L. doing the fabrication, wiring and installation on plants. D.K., N.L., and P.A. designed the maize

dehydration–rehydration experiments. P.A. and M.L.U. performed maize cultivation and plant maintenance. P.A., N.L., and N.K. collected environmental data using commercial sensors.

N.L. collected impedance data; N.L. and U.M. conducted the analysis on the impedance data; N.L. conducted the analysis on the environmental data. M.L.U., U.M., and N.L. designed and conducted the leaf water content (LWC) and sap flow experiments. M.L.U. and N.L. processed and analyzed the LWC and sap flow data. N.L. , U.M., and A.M. conducted the outdoor experiments. N.L. and A.M. processed and analyzed the outdoor experiments data.

N.L. and P.A. designed the leaf pigmentation experiments; N.L. conducted the experiments and performed data analysis. N.L. and P.A. designed the sensor-to-elongation experiments; N.L. conducted the experiments and performed data analysis. N.L. designed the micropore experiments; U.M. conducted the experiments; N.L. analyzed the data. N.L. and U.M. wrote the manuscript with input from all authors.

C.X. provided experimental support and coordinated the maize experiments. D.A., D.K., J.A.I. and H.F supervised the project. D.A., D.K., J.A.I., M.K., H.F., and A.M. provided the research resources and contributed to discussion and interpretation of the results. All authors discussed the results and contributed to revising the manuscript.

References

1. Jones, H. G. Monitoring plant and soil water status: established and novel methods revisited and their relevance to studies of drought tolerance. *J. Exp. Bot.* **58**, 119–130 (2007).

2. Jones, H. G. Irrigation scheduling: advantages and pitfalls of plant-based methods. *J. Exp. Bot.* **55**, 2427–2436 (2004).

3. Yebra, M. *et al.* A global review of remote sensing of live fuel moisture content for fire danger assessment: Moving towards operational products. *Remote Sens. Environ.* **136**, 455–468 (2013).

4. Jiménez-Rodríguez, C. D. *et al.* Detecting Vegetation Stress in Mixed Forest Ecosystems Through the Joint Use of Tree-Water Monitoring and Land Surface Modeling. *Water Resour. Res.* **60**, e2024WR037194 (2024).

5. Bueso, D. *et al.* Soil and vegetation water content identify the main terrestrial ecosystem changes. *Natl. Sci. Rev.* **10**, nwad026 (2023).

6. Yin, S., Ibrahim, H., Schnable, P. S., Castellano, M. J. & Dong, L. A Field-Deployable, Wearable Leaf Sensor for Continuous Monitoring of Vapor-Pressure Deficit. *Adv. Mater. Technol.* **6**, 2001246 (2021).

7. Serrano-Finetti, E., Castillo, E., Alejos, S. & León Hilario, L. M. Toward noninvasive monitoring of plant leaf water content by electrical impedance spectroscopy. *Comput. Electron. Agric.* **210**, 107907 (2023).

8. Baldacci, L. *et al.* Non-invasive absolute measurement of leaf water content using terahertz quantum cascade lasers. *Plant Methods* **13**, 51 (2017).

9. Bukhamsin, A., Kosel, J., Blilou, I. & Salama, K. N. Accelerating adoption of species-agnostic plant sensors for precision farming. *Nat. Rev. Electr. Eng.* **2**, 58–70 (2025).

10. García-Haro, F. J. *et al.* A global Canopy Water Content product from AVHRR/Metop. *ISPRS J. Photogramm. Remote Sens.* **162**, 77–93 (2020).

11. Rodriguez-Dominguez, C. M. *et al.* Leaf water potential measurements using the pressure chamber: Synthetic testing of assumptions towards best practices for precision and accuracy. *Plant Cell Environ.* **45**, 2037–2061 (2022).

12. Quemada, C. *et al.* Remote Sensing for Plant Water Content Monitoring: A Review. *Remote Sens.* **13**, 2088 (2021).

13. Yan, X. *et al.* Wearable Sensors for Plants: Status and Prospects. *Biosensors* **15**, 53 (2025).

14. Luo, Y. *et al.* A Morphable Ionic Electrode Based on Thermogel for Non-Invasive Hairy Plant Electrophysiology. *Adv. Mater.* **33**, 2007848 (2021).

15. Wong, Y. J. *et al.* Adaptable thermoresponsive polymer for long-term electrical coupling in plant electrophysiology monitoring. *Sci. Adv.* **12**, eady1400 (2026).

16. Su, P.-G. & Chiou, C.-F. Electrical and humidity-sensing properties of reduced graphene oxide thin film fabricated by layer-by-layer with covalent anchoring on flexible substrate. *Sens. Actuators B Chem.* **200**, 9–18 (2014).

17. Oren, S., Ceylan, H., Schnable, P. S. & Dong, L. High-Resolution Patterning and Transferring of Graphene-Based Nanomaterials onto Tape toward Roll-to-Roll Production of Tape-Based Wearable Sensors. *Adv. Mater. Technol.* **2**, 1700223 (2017).

18. Zeng, S. *et al.* Ultrafast response of self-powered humidity sensor of flexible graphene oxide film. *Mater. Des.* **226**, 111683 (2023).

19. Misra, U. *et al.* Graphene In-Sensor Compute Device for Plant Hydration Monitoring. *Nano Lett.* **26**, 2432–2440 (2026).

20. Kireev, D. *et al.* Continuous cuffless monitoring of arterial blood pressure via graphene bioimpedance tattoos. *Nat. Nanotechnol.* **17**, 864–870 (2022).

21. Kireev, D. *et al.* Fabrication, characterization and applications of graphene electronic tattoos. *Nat. Protoc.* **16**, 2395–2417 (2021).

22. Akinwande, D. & Kireev, D. Wearable graphene sensors use ambient light to monitor health. *Nature* **576**, 220–221 (2019).

23. Liu, N., Rossi, W., Kireev, D. & Akinwande, D. Electrophysiological Sensing with Graphene Electronic Tattoos for Saline and Underwater Environments. *ACS Appl. Electron. Mater.* **7**, 5868–5875 (2025).

24. Lee, H. *et al.* A non-invasive approach to skin cancer diagnosis via graphene electrical tattoos and electrical impedance tomography. *Physiol. Meas.* **45**, 055003 (2024).

25. Lin, Z. *et al.* Graphene Biointerface for Cardiac Arrhythmia Diagnosis and Treatment. *Adv. Mater.* **35**, 2212190 (2023).

26. Li, D., Li, G., Li, J. & Xu, S. Wearable Crop Sensor Based on Nano-Graphene Oxide for Noninvasive Real-Time Monitoring of Plant Water. *Membranes* **12**, 358 (2022).

27. Zhao, Y. *et al.* Multifunctional Stretchable Sensors for Continuous Monitoring of Long-Term Leaf Physiology and Microclimate. *ACS Omega* **4**, 9522–9530 (2019).

28. Miccoli, I., Edler, F., Pfnür, H. & Tegenkamp, C. The 100th anniversary of the four-point probe technique: the role of probe geometries in isotropic and anisotropic systems. *J. Phys. Condens. Matter* **27**, 223201 (2015).

29. Brantlov, S. *et al.* Cell Membrane Capacitance (Cm) Measured by Bioimpedance Spectroscopy (BIS): A Narrative Review of Its Clinical Relevance and Biomarker Potential. *Sensors* **25**, 4362 (2025).

30. Gabriel, S., Lau, R. W. & Gabriel, C. The dielectric properties of biological tissues: III. Parametric models for the dielectric spectrum of tissues. *Phys. Med. Biol.* **41**, 2271 (1996).

31. Van Haeverbeke, M., De Baets, B. & Stock, M. Plant impedance spectroscopy: a review of modeling approaches and applications. *Front. Plant Sci.* **14**, (2023).

32. Pathare, V. S., Koteyeva, N. & Cousins, A. B. Increased adaxial stomatal density is associated with greater mesophyll surface area exposed to intercellular air spaces and mesophyll conductance in diverse C4 grasses. *New Phytol.* **225**, 169–182 (2020).

33. Jócsák, I., Végvári, G. & Vozáry, E. Electrical impedance measurement on plants: a review with some insights to other fields. *Theor. Exp. Plant Physiol.* **31**, 359–375 (2019).

34. Blackman, C. J., Brodribb, T. J. & Jordan, G. J. Leaf hydraulics and drought stress: response, recovery and survivorship in four woody temperate plant species. *Plant Cell Environ.* **32**, 1584–1595 (2009).

35. Abid, M. *et al.* Improved tolerance to post-anthesis drought stress by pre-drought priming at vegetative stages in drought-tolerant and -sensitive wheat cultivars. *Plant Physiol. Biochem.* **106**, 218–227 (2016).

36. Yang, W. *et al.* Light intensity affects the coloration and structure of chimeric leaves of Ananas comosus var. bracteatus. 2020.10.27.356857 Preprint at https://doi.org/10.1101/2020.10.27.356857 (2020).

37. Sheehy, D. E. & Schmalian, J. Optical transparency of graphene as determined by the fine-structure constant. *Phys. Rev. B* **80**, 193411 (2009).

38. Jang, H., Dai, Z., Ha, K.-H., Ameri, S. K. & Lu, N. Stretchability of PMMA-supported CVD graphene and of its electrical contacts. *2D Mater.* **7**, 014003 (2019).

39. Kireev, D., Kampfe, J., Hall, A. & Akinwande, D. Graphene electronic tattoos 2.0 with enhanced performance, breathability and robustness. *Npj 2D Mater. Appl.* **6**, 46 (2022).

40. Zhou, H. *et al.* Capability of leaf water content and its threshold values in reflection of soil–plant water status in maize during prolonged drought. *Ecol. Indic.* **124**, 107395 (2021).

41. Liu, Y. *et al.* Electrical impedance spectroscopy (EIS) in plant roots research: a review. *Plant Methods* **17**, 118 (2021).

42. Zhou, H. *et al.* Capability of leaf water content and its threshold values in reflection of soil–plant water status in maize during prolonged drought. *Ecol. Indic.* **124**, 107395 (2021).

Supplementary Files

This is a list of supplementary files associated with this preprint. Click to download.

- plantprojectSUPINFO.pdf
- SUPVideo1.mov